Emission of conical THz radiation induced by bichromatic pump X waves in an air plasma

D. Buožius, B. Motiejūnas, V. Vaičaitis, and V. Tamulienė*
Laser Research Center, Vilnius University, LT-10223 Saulėtekio 10, Vilnius, Lithuania

(Received 8 September 2021; accepted 9 February 2022; published 24 February 2022)

The X-wave formation during the propagation of bichromatic femtosecond laser pulses in an air plasma filament and THz radiation generation has been investigated both experimentally and theoretically. We found that in this case the pump waves as well as THz radiation propagate as X waves at the same group velocity. Therefore, the cone angle of generated THz radiation could be estimated using the X-wave dispersion law. Hence, the proposed model allows an alternative characterization of generated THz radiation based on the frequency-angular spectra of pump waves registered after propagation in the created plasma filament.

DOI: 10.1103/PhysRevA.105.023521

I. INTRODUCTION

X waves are important localized structures discovered in numerous disciplines of physics governed by the wave equation: acoustics, electromagnetism, gravitational waves, and others. In electromagnetism, we deal with the superluminal localized pulses [1] that obey the X shape and the linear dispersion relation: $k_z = a\omega + b$. Here, k_z and ω are the longitudinal wave-vector component and angular frequency of the light wave, respectively. a and b are constants. X waves are composed of wave vectors with longitudinal components obeying the same phase velocity. Then, the phase velocity becomes the group velocity and here we refer to this as the X-wave group velocity. Although this velocity exceeds the speed of light, the propagation of X waves does not contradict the physics [1].

Nonlinear X waves [2] were shown to be crucial in the light filamentation of water [3] and air [4]. The formation of a light filament is accompanied by the interplay of dispersion, diffraction, nonlinear Kerr focusing, and plasma defocusing processes. The formation of an X wave just after the nonlinear focus and its propagation with a stationary profile inside the filament were shown [4]. Interestingly, X-wave formation was shown to also appear at tight focusing and third-harmonic generation in air pumped by infrared radiation [5–8]. Both fundamental and third harmonics as well as the generated fifth harmonic were shown to be X waves propagating at the same group velocity [5,8]. Therefore, bearing in mind the findings described above, here we are discussing the following question: What is the influence of the X waves on the terahertz (THz) radiation generated in air by the bichromatic pump?

The THz radiation generated in air plasma excited by the fundamental harmonic (FH) and its second harmonic (SH) was studied in numerous works both experimentally and numerically [9,10]. In most cases, a femtosecond Ti:sapphire laser operating at 800 nm was used in these experiments. The FH and SH are focused by a lens and the plasma channel in the vicinity of the focus is created where the broadband conical THz radiation is generated [11].

Theoretically, the THz emission is described as the radiation generated by a plasma current [12]. Usually, the THz radiation angular spectrum obeys a conical structure. First, this conical emission at terahertz frequency was explained by the mismatch of the phase velocities of the pump waves [13]. Later, this result was compared with the cone angle of the Cherenkov radiation [14] that was calculated knowing the front velocity of the plasma current. In addition, a comprehensive but quite complex physical model including many effects such as the phase change that terahertz radiation gets due to propagation inside the plasma, as well as plasma opacity for radiation with frequencies below its own one was proposed to explain the conical character of broadband terahertz generation from femtosecond two-color laser-induced air plasma filaments [15]. Therefore, here we provide an alternative model of the THz cone formation during bichromatic excitation of air by femtosecond laser pulses.

First, we study how both pump waves transform into X waves due to nonlinear propagation in the air plasma. Next, we show that the emitted THz wave can also be described as an X wave. Finally, all three X waves—FH, SH, and THz—are shown to propagate at the same group velocity. Therefore the proposed model allows the estimation of the THz cone angle from either numerically calculated or experimentally measured output pump spectra.

The rest of the paper is organized as follows. In Secs. II and III, we provide the experimental and theoretical methods, respectively. In Sec. IV, the main results are described and discussed. The conclusions are drawn in Sec. V.

II. GENERATION OF THz RADIATION WITH BICHROMATIC PUMP IN AIR

Experimental setup

For our experiment, we have used a Legend elite duo HE+, Coherent Inc. Ti:sapphire chirped pulse amplification laser system providing 40–45 fs [full width at half maximum

*viktorija.tamuliene@ff.vu.lt

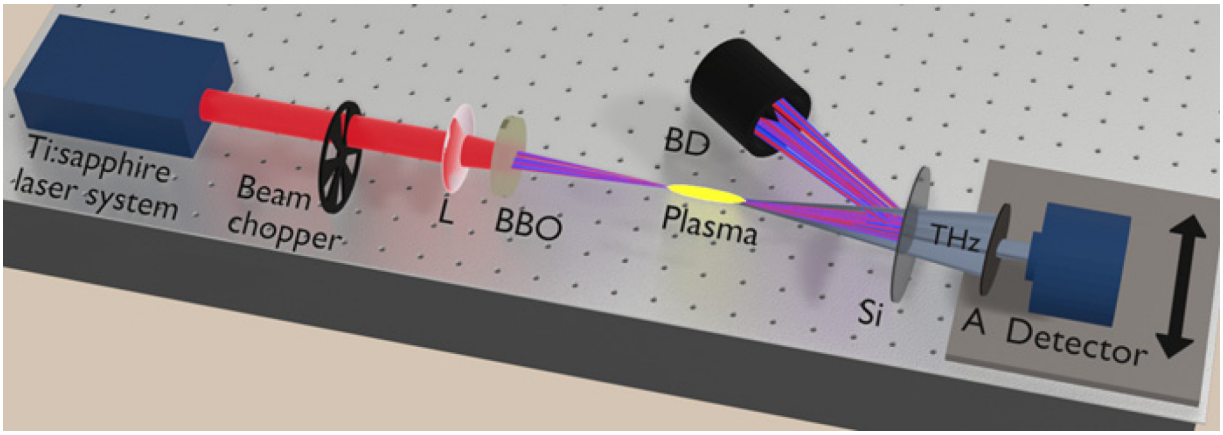

FIG. 1. Schematic of the experimental setup. L: focusing lens; BBO: second-harmonic generation crystal; BD: beam dump; Si: silicon wafer; A: aperture.

(FWHM)] pulses with a central wavelength of 795 nm and a maximum pulse energy of 8 mJ. The repetition rate of the laser system is 1 kHz. The laser power used in the experiment was adjusted using an attenuator consisting of a half-wave plate and a Brewster-type polarizer. The laser beam was focused using a lens L with a focal length of 20 cm. After the lens, the converging beam passes through a 0.2-mm-thick nonlinear beta barium borate (BBO) crystal and generates the second harmonic. Then both of the beams generated an air plasma filament in which THz radiation is being generated.

When measuring the visible light spectrum the pulse energy used for the SH and plasma filament generation was 1.2 mJ. Light diverging from the plasma filament is reflected with a prism towards the optic fiber of the spectrometer placed in total at about 50 cm from the center of the plasma filament. The surface of the prism is used for reflection to reduce the optical power of light reaching the detector while also avoiding multiple reflections from several surfaces. For an additional reduction of light entering the detector, several neutral optical filters are also used. When measuring the spectra of SH, an additional blue colored glass filter was introduced to filter out the fundamental harmonic. Then the optical fiber of the spectrometer is being translated perpendicularly across the beam path on a motorized step motor line where multiple spectra are taken at each of the different positions of the optical fiber [16]. The results of these measurements will be shown in Sec. IV.

When measuring the THz emission cone a similar setup was used. After the plasma, there was a silicon wafer introduced that separates visible light (FH and SH pulses) from the THz radiation. Then to measure the THz signal we used a pyroelectric detector TPR-A-65 THz (Spectrum Detector, Inc.), sensitive in the range 0.1–300 THz (3000–1 μm) with a flat response function from $\approx$3 to $\approx$100 THz. In order to resolve the angular dependence of THz beam intensity we have introduced an aperture of 5 mm diameter in front of the detector. Both the detector and aperture were placed on the step motor driven translation stage that moved perpendicularly to the axis of the initial unfocused beam. In this assembly, we also used a beam chopper to increase the THz signal in comparison to the noise level in a lock-in amplifier. The schematic of this experimental setup is represented in Fig. 1.

III. NUMERICAL SIMULATION OF THE GENERATION OF THz RADIATION

A. Governing equations

The propagation of the focused bichromatic pump in air is described by the unidirectional pulse propagation equation in the Fourier domain,

$$\frac{\partial \widehat{\mathcal{E}}}{\partial z} = iK_z\widehat{\mathcal{E}} + i\widehat{P}_{\text{Kerr}} - i\widehat{P}_{\text{pl}} - \widehat{P}_{\text{loss}}, \tag{1}$$

where $\widehat{\mathcal{E}}(\omega, \beta_x, \beta_y, z)$ is the Fourier transform of the analytical signal $\mathcal{E}(t, x, y, z)$, t is time, and x, y, z are the Cartesian coordinates. The electric field $E = \text{Re}(\mathcal{E})$, where Re($\circ$) is the real part. Next, we describe each term of Eq. (1).

Linear propagation term $iK_z\widehat{\mathcal{E}}$. For fundamental wave and higher harmonics, $K_z = k(\omega) - \beta^2/(2k_{j0}) - \omega/u_{10}$, where $j = 1, 2, 3$ for the fundamental harmonic (FH), second harmonic (SH), and third harmonic (TH), respectively. The frequency interval is divided into equal intervals, e.g., the FH interval is $0.5\nu_{10} < \nu < 1.5\nu_{10}$, while the SH interval is $1.5\nu_{10} < \nu < 2.5\nu_{10}$, where $\nu_{10} = c/\lambda_{10}$ is the FH frequency, λ_{10} is the fundamental wavelength, and c is the speed of light. $k = \frac{\omega}{c}n(\lambda)$ is the wave number and k_{j0} is the wave number of the jth harmonic. $n(\lambda)$ is the wavelength-dependent refractive index of air found by the use of the Sellmeier equation from Ref. [17]. u_{10} is the FH group velocity and the shift ω/u_{10} corresponds to the propagation in the fundamental pulse reference frame. For the terahertz (THz) wave, $K_z = [k^2(\omega) - \beta^2]^{1/2} - \omega/u_{10}$.

Nonlinear $\chi^{(3)}$ *term* $i\widehat{P}_{\text{Kerr}}$. The third-order nonlinear term is given by $\widehat{P}_{\text{Kerr}} = \frac{4}{3}n_2\varepsilon_0\omega\text{F}[\text{Re}(\mathcal{E})^3]$, where F[$\circ$] is the Fourier transform operation, $n_2 = 4 \times 10^{-23}$ m^2/W is the nonlinear refractive index of air, and ε_0 is the vacuum permittivity.

Plasma term $-i\widehat{P}_{\text{pl}}$. The plasma influence is accounted for by $\widehat{P}_{\text{pl}} = \frac{q_e^2}{2m_e c\varepsilon_0}\frac{1}{\omega + i\nu_c}\text{F}[\rho\mathcal{E}]$, where ρ is the plasma density and ν_c is the collision frequency, $\nu_c = 1/200$ fs^{-1} [18]. q_e and m_e are the electron charge and mass, respectively.

Loss term $-\widehat{P}_{\rm loss}$. The nonlinear losses in the plasma are found from

$$\widehat{P}_{\rm loss} = {\rm F}\left[[0.2W_{\rm O}(t)U_{\rm O} + 0.8W_{\rm N}(t)U_{\rm N}]\frac{\rho_0 - \rho}{{\rm Re}(\mathcal{E})2\varepsilon_0 c}\right], \quad (2)$$

where $U_{\rm O}$ and $U_{\rm N}$ are the ionization energies of the main constituents of air—oxygen and nitrogen, respectively. $W(t)$ is the photoemission rate. ρ_0 is the neutral density of air.

The nonlinear propagation terms $\widehat{P}_{\rm Kerr}$, $\widehat{P}_{\rm pl}$, and $\widehat{P}_{\rm loss}$ were calculated at $\omega > 0$.

Plasma density. Both plasma and loss terms $P_{\rm pl}$ and $P_{\rm loss}$ contain the plasma density evolution which is described by the following equation:

$$\frac{\partial \rho}{\partial t} = (\rho_0 - \rho)W(t). \quad (3)$$

For the estimation of the photoemission rate, we utilize the Yudin-Ivanov formula [19]. We note that this formula embraces both multiphoton and tunnel ionization processes. However, it holds only for a single-frequency electromagnetic wave. Therefore, we insert $\mathcal{E}_1$ instead of $\mathcal{E}$ into the formula that is provided by Eq. (15) in Ref. [8]. The Fourier transform $\widehat{\mathcal{E}}_1$ is obtained by truncating $\widehat{\mathcal{E}}$ in the FH frequency domain.

B. Input waves and simulation parameters

At $z = 0$, the input wave consists of focused FH and SH:

$$\begin{aligned}\mathcal{E}(t,x,y,z=0) = {} & E_0 \exp\left(-(x^2+y^2)\left[\frac{1}{r_{10}^2} + \frac{i\pi}{\lambda_{10} f}\right]\right) \\ & \times \exp\left(-\frac{t^2}{\tau^2}\right)\exp(-i\omega_{10}t) \\ & + E_0 m \exp\left(-(x^2+y^2)\left[\frac{1}{r_{20}^2} + \frac{i\pi}{\lambda_{20} f}\right]\right) \\ & \times \exp\left(-\frac{t^2}{\tau^2}\right)\exp(-i\omega_{20}t). \quad (4)\end{aligned}$$

Here, f is the focal length of the lens, and τ is the pulse duration. r_{j0}, λ_{j0}, and ω_{j0} are the FH ($j = 1$) and SH ($j = 2$) beam radius, wavelength, and angular frequency, respectively. E_0 is the input amplitude and m denotes the fraction of the SH amplitude to the FH.

Equation (1) was simulated with the boundary condition Eq. (4) by the use of the symmetrized split-step Fourier transform method [20]. In the vicinity of focus, the longitudinal step was $f/80\,000$ and it was $f/1000$ elsewhere. The vicinity of focus is defined as the interval $0.9f < z < 1.02f$. The cylindrical symmetry was assumed and the fast Hankel transform was utilized [21]. In the time domain, a fast Fourier transform was used. The domain of the radial coordinate $r = \sqrt{x^2+y^2} \in (0,\ 2r_{10})$ was divided into 800 steps and the time domain $t \in [-4\tau,\ 4\tau)$ was divided into 2048 equal steps. The parameters were $\lambda_{10} = 800$ nm, $\lambda_{20} = 400$ nm, $f = 20$ cm, $2r_{10} = 6$ mm, and $r_{20}/r_{10} = 0.5$, $\tau = 30$ fs. The input energy was 150 μJ and the fraction $m^2 = 0.1$.

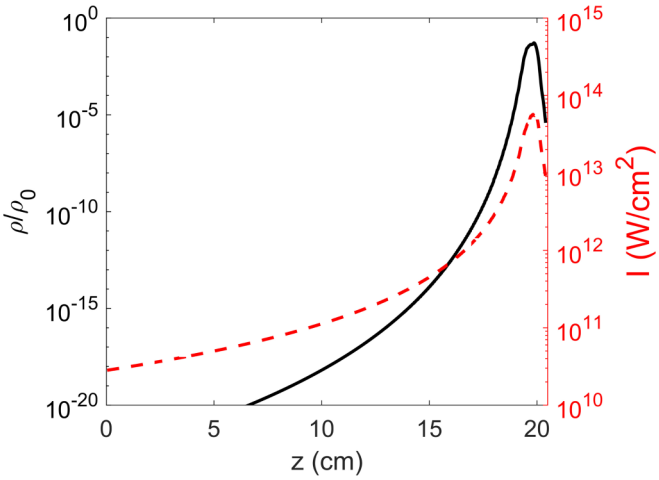

FIG. 2. Dependences of the plasma density (solid black line) and FH intensity (dashed red line) on the propagation distance. Numerical results.

IV. RESULTS AND DISCUSSION

At the given parameters, the FH intensity saturates at around 6×10^{13} W/cm^2 and in the plasma filament, the plasma density ratio to the neutral density is around 0.05 (Fig. 2). From the Marburger's formula [22] we estimated the self-focusing (collapse) distance $z_c = 7.8$ m. The Rayleigh length is $z_R = 35.3$ m, critical power $P_c = 2.4$ GW, and the input power $P_{\rm in} = 4$ GW. From the formula $1/f_c = 1/f + 1/z_c$ we find the effective focus length $f_c = 19.5$ cm.

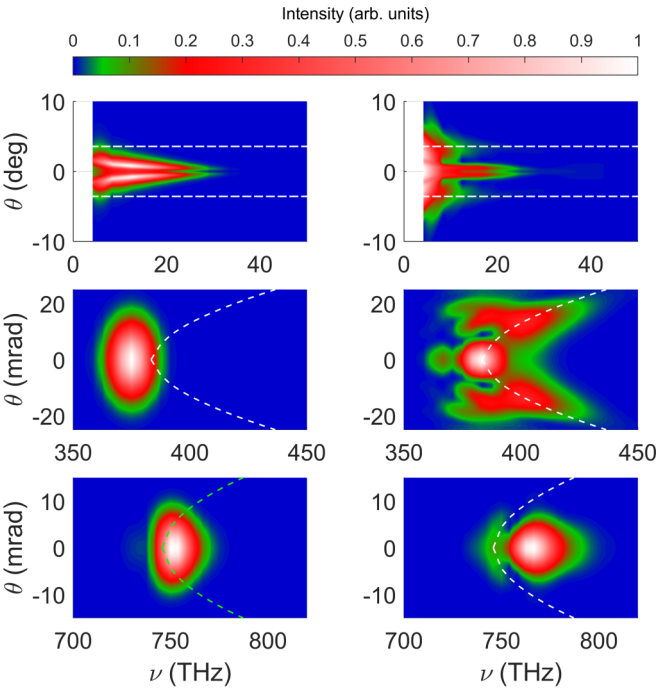

FIG. 3. X-wave dispersion law curves (dashed lines) over the THz (top), FH (center), and SH (bottom) spectra. Left: Before the focus, $z = 18.8$ cm; right: at the output, $z = 20.4$ cm. $U = 3.005 \times 10^8$ m/s. Numerical results. See Supplemental Material [23] for the animated version of the figure.

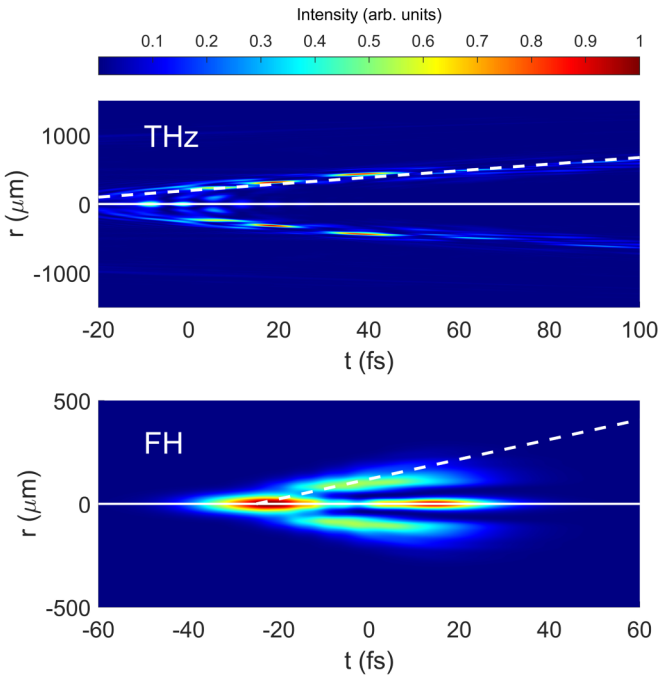

FIG. 4. Output intensity profiles at THz and FH frequencies at $z = 20.4$ cm. The slope of the dashed line: $\pi/2 - \theta_{\mathrm{THz}}$. Numerical results.

In Fig. 3, we depict the spectra of the three waves—THz, FH, and SH—in the ν, θ plane, e.g., the frequency-angle plane. The output FH and SH spectra are modified and the part of the emission is conical. This conical emission may be attributed to the X waves propagating at the same group velocity both for FH and SH. The X-wave dispersion law reads [8]

$$k_{1,2}(\omega)\cos(\theta) = \frac{\omega - \omega_{1,20}}{U} + k_{1,20}, \tag{5}$$

where U is the group velocity of the X wave. This dispersion law fits well the calculated spectra when $U = 3.005 \times 10^8$ m/s and the dispersion curves are depicted by the dashed lines in Fig. 3 (center and bottom graphs). The X-wave dispersion law may also be formulated for the THz radiation,

$$\cos(\theta) = \frac{v_{\mathrm{THz}}(\omega)}{U}, \tag{6}$$

where $v_{\mathrm{THz}}(\omega)$ is the phase velocity of the THz radiation. Here, we assumed that the THz conical X wave propagates with the same group velocity U as the pump X waves. To confirm this assumption we depict the dispersion curve of Eq. (6) by the dashed line in Fig. 3 (top). This dashed line corresponds to an approximately constant cone angle $\theta_{\mathrm{THz}} = 3.58^\circ$ and it fits the depicted output THz spectrum well. The group velocity U of the FH and SH was inserted into Eq. (6).

Comparing the left and right graphs in Fig. 3 one can see that at the onset of the plasma filament both the pump X waves and the THz conical emission are absent. At the output, the conical THz emission appears and the pump X waves are observed as well. The animation (see Supplemental Material [23] for the animated version of Fig. 3) shows the details of this transition: The THz cone appears at the onset of the pump X-wave formation. Further, the pump spectrum is stationary while the THz cone becomes more visible. We note that a longer plasma filament supports both the X-wave formation [4] and THz generation [12].

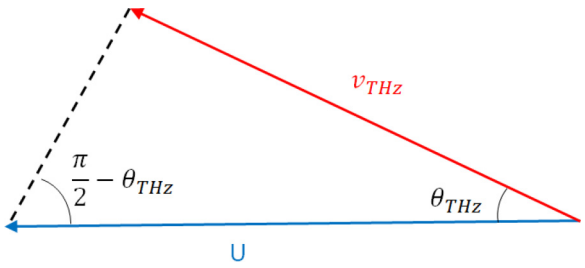

FIG. 5. Scheme of X-wave group velocity and THz phase velocity vectors.

The X-wave dispersion law for THz wave resembles the Cherenkov's formula for the optical Cherenkov's emission angle ϕ [14],

$$\cos(\phi) = \frac{v_{\mathrm{THz}}(\omega)}{v_f}, \tag{7}$$

where v_f is the plasma current front velocity. We note that the Cherenkov's radiation angle is closely related to the angle

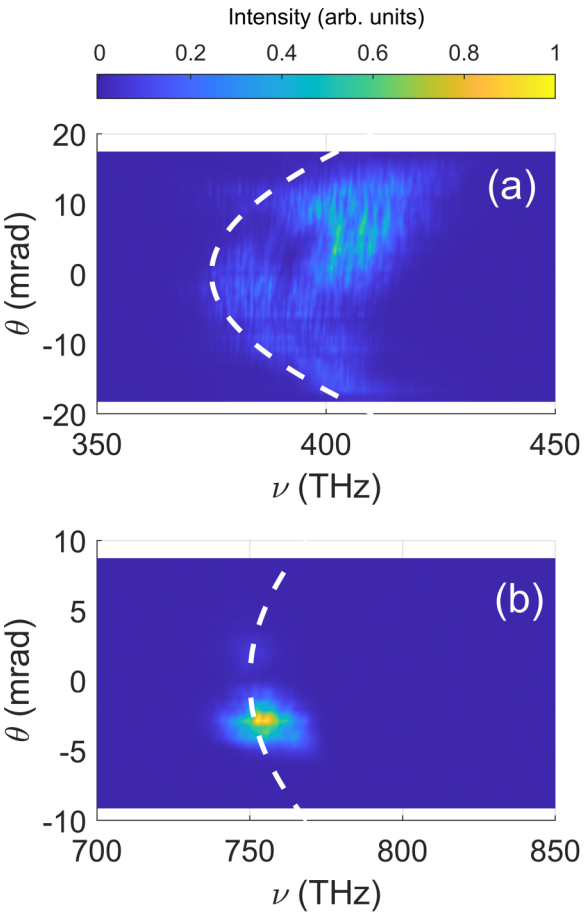

FIG. 6. Registered spectra of (a) FH and (b) SH waves. Dashed lines: The same dispersion law as in Fig. 3. Experimental results.

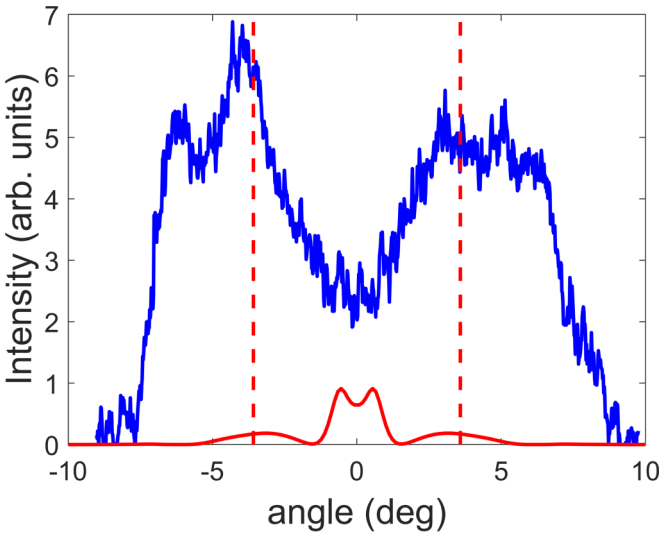

FIG. 7. Experimentally registered THz cone (blue line). Red solid line: Theoretically simulated THz angular distribution at $\nu =$ 12 THz. Red dashed line: $\theta_{\mathrm{THz}} = 3.58^{\circ}$.

estimated from the slope of the field profile at terahertz frequencies [14]. In Fig. 4 (top), the dashed line with the slope $\pi/2 - \theta_{\mathrm{THz}}$ shows that the Cherenkov's angle ϕ should be close to the estimated cone angle for the terahertz X wave θ_{THz}. This dashed line fits the intensity profile of the FH as well [Fig. 4 (bottom)]. In the case of the X wave, the vectors of the group velocity U and THz phase velocity v_{THz} make an angle θ_{THz} (Fig. 5).

Previously, You *et al.* [13] noted that the conical nature of the THz emission is due to the phase velocity mismatch of the pump waves. On the other hand, in Ref. [14], the authors showed that their prediction based on the Cherenkov's effect gives a similar result. In both Refs. [13,14], the plasma term was included in the refractive index. However, in this work, we do not include the plasma term in the refractive index [in Eq. (6)] since the dispersion curves with output spectra at low plasma density are compared. But the plasma influence is accounted for in the numerical simulations [Eq. (1)] and it is prominent at the vicinity of the focus when the intensity clamping takes place.

Finally, in Fig. 6 the experimentally registered spectra of FH and SH are depicted and the dashed lines correspond to the dispersion law of Eq. (5) with the theoretical value of group velocity U. The FH X wave is clearly visible while the SH X wave lacks the contrast in the measured data. The registered THz cone is presented in Fig. 7 and the theoretical angle value θ_{THz} is noted by the red dashed line. Here, the theoretically simulated THz angular distribution at 12 THz is also depicted. The cone at angle θ_{THz} can be seen.

Note that recently it was suggested that the conical THz emission could be a result of photoinduced carriers in the silicon wafer, used to block the remaining pump laser light [24]. However, this effect was demonstrated in the case of low-frequency THz beams, while in our experiment most of the THz pulse energy was contained in the high-frequency part of the THz radiation. Nevertheless, the influence of photoinduced carriers could explain the large angular spread of the off-axis THz radiation shown in Fig. 7.

V. CONCLUSIONS

In conclusion, we demonstrated that during THz radiation generation in air by bichromatic femtosecond laser pulses both pump waves are modified due to the nonlinear propagation in the plasma filament and their output frequency-angular spectra can be described by the X-wave dispersion law with the same group velocity. The emitted THz wave is shown to follow an X-wave dispersion law with the group velocity of the pump X waves. The group velocity was estimated from the frequency-angular spectra of the pump waves. The THz cone angle was calculated from the dispersion law where the estimated pump X-wave group velocity was inserted. Both theoretical and experimental data confirm the predicted relation between the pump X-wave group velocity and THz cone angle. This allows the characterization of the angular structure of generated THz radiation based on the properties of the output pump waves.

ACKNOWLEDGMENT

This research was funded by a grant (No. S-MIP-19-46) from the Research Council of Lithuania.

[1] E. Recami, M. Zamboni-Rached, and H. E. Hernández-Figueroa, Localized waves: A historical and scientific introduction, in *Localized Waves* (Wiley, Hoboken, NJ, 2008), Chap. 1, pp. 1–41.

[2] C. Conti and S. Trillo, Nonlinear X-waves, in *Localized Waves* (Wiley, Hoboken, NJ, 2008), Chap. 9, pp. 243–272.

[3] M. Kolesik, E. M. Wright, and J. V. Moloney, Dynamic Nonlinear X Waves for Femtosecond Pulse Propagation in Water, Phys. Rev. Lett. **92**, 253901 (2004).

[4] D. Faccio, A. Averchi, A. Lotti, P. Di Trapani, A. Couairon, D. Papazoglou, and S. Tzortzakis, Ultrashort laser pulse filamentation from spontaneous X Wave formation in air, Opt. Express **16**, 1565 (2008).

[5] H. Xu, H. Xiong, Y. Fu, J. Yao, Z. Zhou, Y. Cheng, Z. Xu, and S. L. Chin, Formation of X-waves at fundamental and harmonics by infrared femtosecond pulse filamentation in air, Appl. Phys. Lett. **93**, 241104 (2008).

[6] H. Xiong, H. Xu, Y. Fu, Y. Cheng, Z. Xu, and S. L. Chin, Spectral evolution of angularly resolved third-harmonic generation by infrared femtosecond laser-pulse filamentation in air, Phys. Rev. A **77**, 043802 (2008).

[7] H. Xu, H. Xiong, R. Li, Y. Cheng, Z. Xu, and S. L. Chin, X-shaped third harmonic generated by ultrashort infrared pulse filamentation in air, Appl. Phys. Lett. **92**, 011111 (2008).

[8] V. Tamulienė, G. Juškevičiūtė, D. Buožius, V. Vaičaitis, I. Babushkin, and U. Morgner, Influence of tunnel ionization to third-harmonic generation of infrared femtosecond laser pulses in air, Sci. Rep. **10**, 17437 (2020).

[9] D. J. Cook and R. M. Hochstrasser, Intense terahertz pulses by four-wave rectification in air, Opt. Lett. **25**, 1210 (2000).

[10] C. Tailliez, A. Stathopulos, S. Skupin, D. Buožius, I. Babushkin, V. Vaičaitis, and L. Bergé, Terahertz pulse generation by two-color laser fields with circular polarization, New J. Phys. **22**, 103038 (2020).

[11] H. Zhong, N. Karpowicz, and X.-C. Zhang, Terahertz emission profile from laser-induced air plasma, Appl. Phys. Lett. **88**, 261103 (2006).

[12] V. Andreeva, O. Kosareva, N. Panov, D. Shipilo, P. Solyankin, M. Esaulkov, P. González de Alaiza Martínez, A. Shkurinov, V. Makarov, L. Bergé, and S. Chin, Ultrabroad Terahertz Spectrum Generation from an Air-Based Filament Plasma, Phys. Rev. Lett. **116**, 063902 (2016).

[13] Y. S. You, T. I. Oh, and K. Y. Kim, Off-Axis Phase-Matched Terahertz Emission from Two-Color Laser-Induced Plasma Filaments, Phys. Rev. Lett. **109**, 183902 (2012).

[14] L. A. Johnson, J. P. Palastro, T. M. Antonsen, and K. Y. Kim, THz generation by optical Cherenkov emission from ionizing two-color laser pulses, Phys. Rev. A **88**, 063804 (2013).

[15] A. Gorodetsky, A. D. Koulouklidis, M. Massaouti, and S. Tzortzakis, Physics of the conical broadband terahertz emission from two-color laser-induced plasma filaments, Phys. Rev. A **89**, 033838 (2014).

[16] V. Vaičaitis, M. Kretschmar, R. Butkus, R. Grigonis, U. Morgner, and I. Babushkin, Spectral broadening and conical emission of near-infrared femtosecond laser pulses in air, J. Phys. B: At., Mol. Opt. Phys. **51**, 045402 (2018).

[17] P. E. Ciddor, Refractive index of air: New equations for the visible and near infrared, Appl. Opt. **35**, 1566 (1996).

[18] V. Yu. Fedorov and S. Tzortzakis, Extreme THz fields from two-color filamentation of midinfrared laser pulses, Phys. Rev. A **97**, 063842 (2018).

[19] G. L. Yudin and M. Y. Ivanov, Nonadiabatic tunnel ionization: Looking inside a laser cycle, Phys. Rev. A **64**, 013409 (2001).

[20] M. S. Wartak, *Computational Photonics. An Introduction with MATLAB* (Cambridge University Press, Cambridge, U.K., 2013), pp. 357–360.

[21] P. Banerjee, G. Nehmetallah, and M. Chatterjee, Numerical modeling of cylindrically symmetric nonlinear self-focusing using an adaptive fast Hankel split-step method, Opt. Commun. **249**, 293 (2005).

[22] A. Couairon, E. Brambilla, T. Corti, D. Majus, O. de J. Ramírez-Góngora, and M. Kolesik, Practioner's guide to laser pulse propagation models and simulation, Eur. Phys. J.: Spec. Top. **199**, 5 (2011).

[23] See Supplemental Material at http://link.aps.org/supplemental/10.1103/PhysRevA.105.023521 for the animated version of Fig. 3.

[24] C. B. Sørensen, L. Guiramand, J. Degert, M. Tondusson, E. Skovsen, E. Freysz, and E. Abraham, Conical versus Gaussian terahertz emission from two-color laser-induced air plasma filaments, Opt. Lett. **45**, 2132 (2020).